Title
Modeling And Control Design For A Computer Controlled Brake System

Authors
Raza, H.
Xu, Z.
Ioannou, P.
et al.

Publication Date
1995

CALIFORNIA PATH PROGRAM
INSTITUTE OF TRANSPORTATION STUDIES
UNIVERSITY OF CALIFORNIA, BERKELEY

Modeling and Control Design for a Computer Controlled Brake System

H. Raza, Z. Xu, P. Ioannou, B. Yang
University of Southern California

California PATH Research Report
UCB-ITS-PRR-95-37

This work was performed as part of the California PATH Program of the University of California, in cooperation with the State of California Business, Transportation, and Housing Agency, Department of Transportation; and the United States Department of Transportation, Federal Highway Administration.

Report for MOU 57

November 1995

ISSN 1055-1425

Modeling and Control Design for a Computer Controlled Brake System*

H. Raza, Z. Xu and P. Ioannou
Dept. of Electrical Engineering-Systems
University of Southern California
Los Angeles, CA 90089-2563
(213)740-4452

Abstract. The brake subsystem is one of the most significant parts of a vehicle with respect to safety. A computer controlled brake system has the capability of acting faster than the human driver during emergencies, and therefore has the potential of improving safety.

In this paper we consider the problem of modeling and control of a computer controlled brake system. The brake model is developed using a series of experiments conducted on a test bench which contains the full scale brake subsystem of a Lincoln town car† and a computer controlled actuator designed by Ford Motor Company. The developed model has the form of a first order nonlinear system with the system nonlinearities lumped in the model coefficients. The unknown model parameters are identified by applying curve fitting techniques to the experimental data. The major characteristics of the system input-output curves such as time delay, effect of static friction, transient and steady state parts, have been identified in terms of model parameters. The brake controller design makes use of a standard feedback linearization technique along with intuitive modifications to meet the closed loop performance specifications. The simulation results show that the proposed controller guarantees no overshoot and zero steady state error for step inputs. Test of the same controller using the experimental bench setup demonstrates its effectiveness in meeting the performance requirements.

Keywords: Modeling, Brake System, Discrete Time Control, Feedback Linearization, Advanced Vehicle Control Systems, Automated Highway Systems.

*This work is supported by the California Department of Transportation through PATH of the University of California and Ford Motor Company. The contents of this paper reflect the views of the authors who are responsible for the facts and the accuracy of the data presented herein. The contents do not necessarily reflect the official views or policies of the State of California. This paper does not constitute a standard, specification or regulation.

†Lincoln town car is the trade mark of Ford Motor Company

Executive Summary

In this paper the problem of modeling and control design of a computer controlled brake system is addressed. The brake system under consideration is a test bench designed by Ford Motor Company, which contains the full scale brake subsystem of Lincoln Town car and a computer controlled actuator.

A nonlinear model for the brake system is developed by analyzing the input-output data obtained from the test bench. The model identifies the major characteristics of the brake system, such as time delay, transient and steady state behavior. The model can be used in designing and testing vehicle brake controllers and in calculating safe inter-vehicle spacings by tking into account the time delay of the brake system.

A controller for the brake system is designed by applying feedback linearization technique along with intuitive modifications to meet the closed loop performance specifications. The simulation results show that the proposed controller guarantees no overshoot and zero steady state error for step inputs. Test of the same controller using the experimental bench setup demonstrates its effectiveness in meeting the performance requirements.

Contents

List of Figures

List of Tables

1 Introduction

With an ever-increasing number of vehicles on the limited highways, it has become urgent to develop sophisticated technical solutions to today's surface transportation problems. Intelligent Transportation Systems (ITS) is an area whose purpose is to improve the efficiency of the current transportation system through the use of advanced technologies. These technologies will be used to automate vehicles, infrastructure and improve the intelligence of decision making. An important part of ITS is the Advanced Vehicle Control Systems (AVCS) whose purpose is to improve safety and vehicular traffic flow rates by automating some or all of the basic functions of the vehicle, i.e., throttle, brake and steering control.

In this paper we consider the computer controlled brake subsystem function. The objective is to understand the dynamics of the braking function by modeling its behavior as a dynamic system and to design and test control algorithms for controlling it in order to meet given performance requirements.

During the past few years, several attempts have been made by different research groups to develop models of the brake subsystem for AVCS applications. One such important contribution is the work of Gerdes et. al. [6]. A bond graph method for modeling the components of manual brake system is considered in the paper by Khan, Kulkarni and Yocef-Toumi [7]. In these studies the emphasis was given on identifying the dynamics associated with each brake component. A comprehensive dynamic model of the brake subsystem for AVCS applications, which identifies the mapping from input to output, has not been addressed. The main purpose of this paper is to develop a model and a controller for brake subsystem that can be used in AVCS applications.

The brake model is developed using an experimental set up on a bench of the full scale Lincoln town car brake subsystem. The block diagram of the brake subsystem under study is shown in Figure 1. The test bench has all the conventional brake components, in addition, it contains an auxiliary hydraulic module (AHM) which consists of a hydraulic pump, control valves and an actuator. It has been designed by Ford specifically for automatic brake applications. This design allows the driver to override at any time.

The dynamic system or model describing the input-output behavior of the brake subsystem is developed by using a series of experiments and curve fitting techniques to identify the unknown parameters. The resulting model is a first order nonlinear dynamic system that accurately describes the dynamics of the actual brake subsystem.

The brake model is used to design a controller that can meet the given performance and reliability requirements. The controller employs feedback linearization to cancel the nonlinearities and a modified proportional integral (PI) compensator to achieve the desired control action. The modeling and control techniques used in this paper can be easily

applied to other types of brake subsystems with minor modifications. Other brake control strategies which are used as part of vehicle longitudinal controllers can be found in [10]-[11].

The paper is organized as follows:
Section 2 describes briefly the structure of the brake subsystem components. For more detailed descriptions the reader is referred to [8], [6]. The brake subsystem model is developed in section 3. In section 4 we consider the problem of identification of the unknown model parameters. This is followed by simulation results and model validation. The control design with the modification logic for the PI compensator is given in section 5. In section 6 the stability properties of the controller and some robustness issues are discussed briefly. The controller implementation and simulation results are given in section 7.

2 Brake System Components

The main components of the brake subsystem shown in Figure 1 are discussed below.

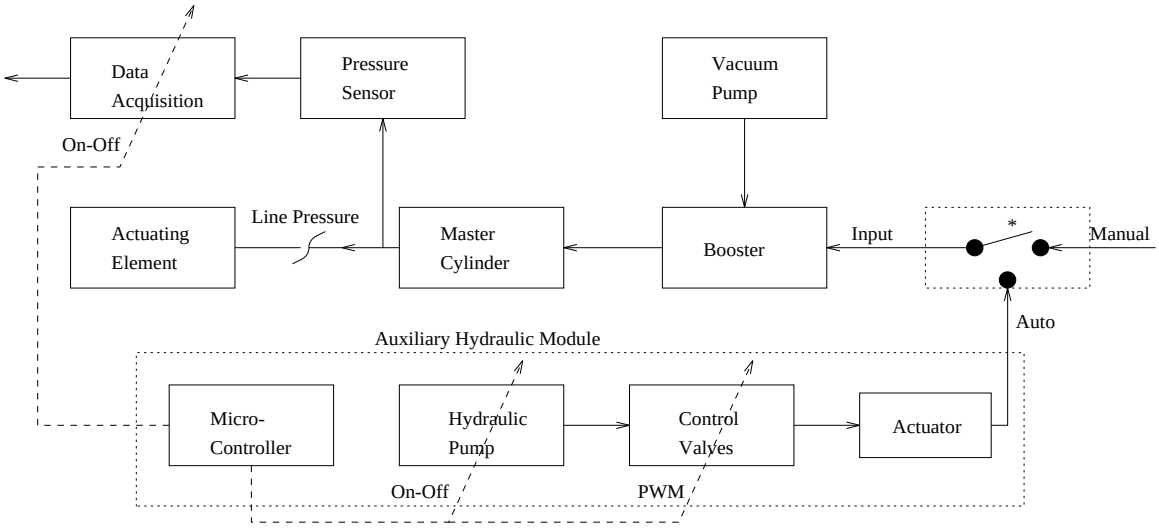

Figure 1: Block Diagram of the Brake Subsystem

2.1 Auxiliary Hydraulic Module

The function of the AHM is to provide an input force to the vacuum booster through an actuator and brake pedal. The AHM takes the control input in the form of a pulse width modulated (PWM) signal and generates a pressure to be applied to the brake pedal through an actuator. The PWM signal is in the form of a square wave of fixed frequency but varying

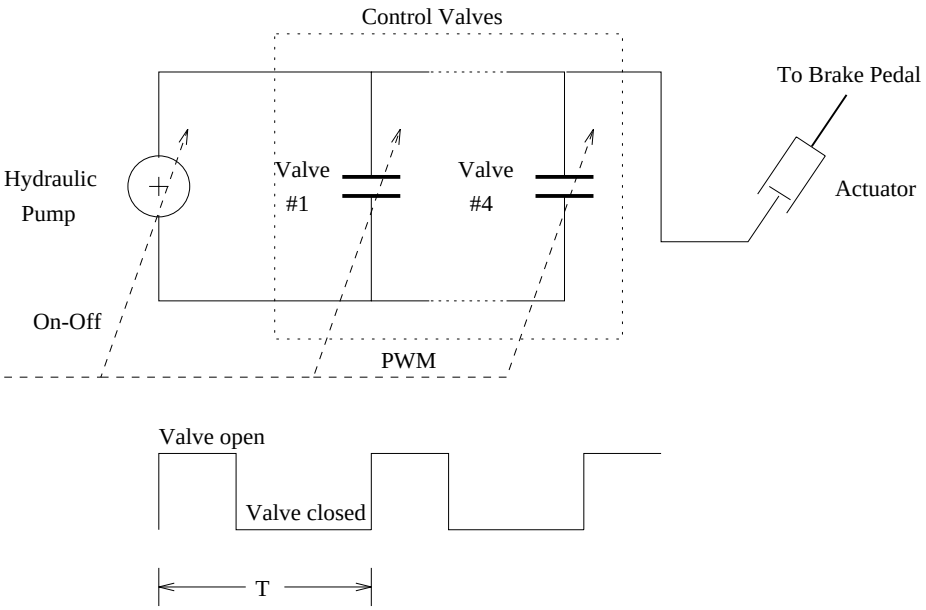

Figure 2: Block Diagram of the Auxiliary Hydraulic Module

duty cycle. The output pressure of the actuator and hence the brake line pressure can be controlled by changing the duty cycle of the PWM signal.

As shown in Figure 2 the AHM consists of a hydraulic pump, an arrangement of valves and an actuator. When a constant amount of fluid is pumped through the valves by the hydraulic pump, no pressure is developed inside the cylinder of the actuator if the valves are open. Whereas a sudden rise of pressure is obtained if the valves are closed completely. Hence an average amount of pressure can be maintained inside the cylinder of the actuator by switching the valves at high frequency (typically 100 Hz) with changeable duty cycle (percentage of valve open time in one switching period). This pressure pushes the piston of the actuator and applies force to the brake pedal.

When the duty cycle is changed, the pressure inside the cylinder of the actuator changes too. Hence the force applied to the brake pedal can be controlled by varying the duty cycle of the PWM signal. It should be noted that the maximum value of duty cycle corresponds to valves being open for most of the time and hence no force is applied to the brake pedal, which results in minimum brake line pressure at the output of the master cylinder. From the overall system point of view any permissible pressure value at the output of the master cylinder can be obtained by some particular value of duty cycle. The model developed in this paper identifies the mapping from duty cycle to the line pressure.

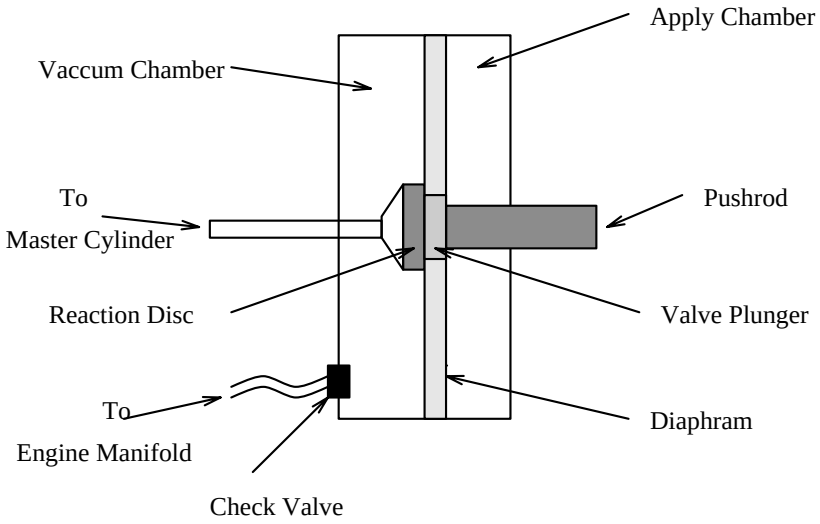

Figure 3: Block Diagram of the Vacuum Booster

2.2 Vacuum Booster

A simplified diagram of the vacuum booster is shown in Figure 3. The force amplification is caused by a pressure differential between the apply and vacuum chambers. Ideally, the amplification ratio between the input and output forces should be constant over the recommended range of operation. However, due to booster dynamics this ratio is not constant. According to the operation of the booster each brake application operation can be broken down into three basic stages: stage 1: apply; stage 2: hold or lap; stage 3: release. These stages are shown in Figure 4.

• In the apply stage control valve moves forward, the atmospheric valve is opened and the vacuum valve is closed, hence a pressure differential is created, causing the diaphragm to move forward.
• When the diaphragm travels further, the valve housing catches up with the control valve. This movement also closes the atmospheric valve. The diaphragm and the valve body are now in the hold stage.
• When the brake pedal is released, the control valve moves back due to the spring force, the apply and vacuum chambers are connected and the pressure differential is reduced to zero.

Since the inertia of the push rod and diaphragm is quite significant, the associated dynamics can not be neglected. Furthermore, the changes of pressure in the apply and vacuum chambers also give rise to thermodynamics. For more detailed discussion of these effects, see [6].

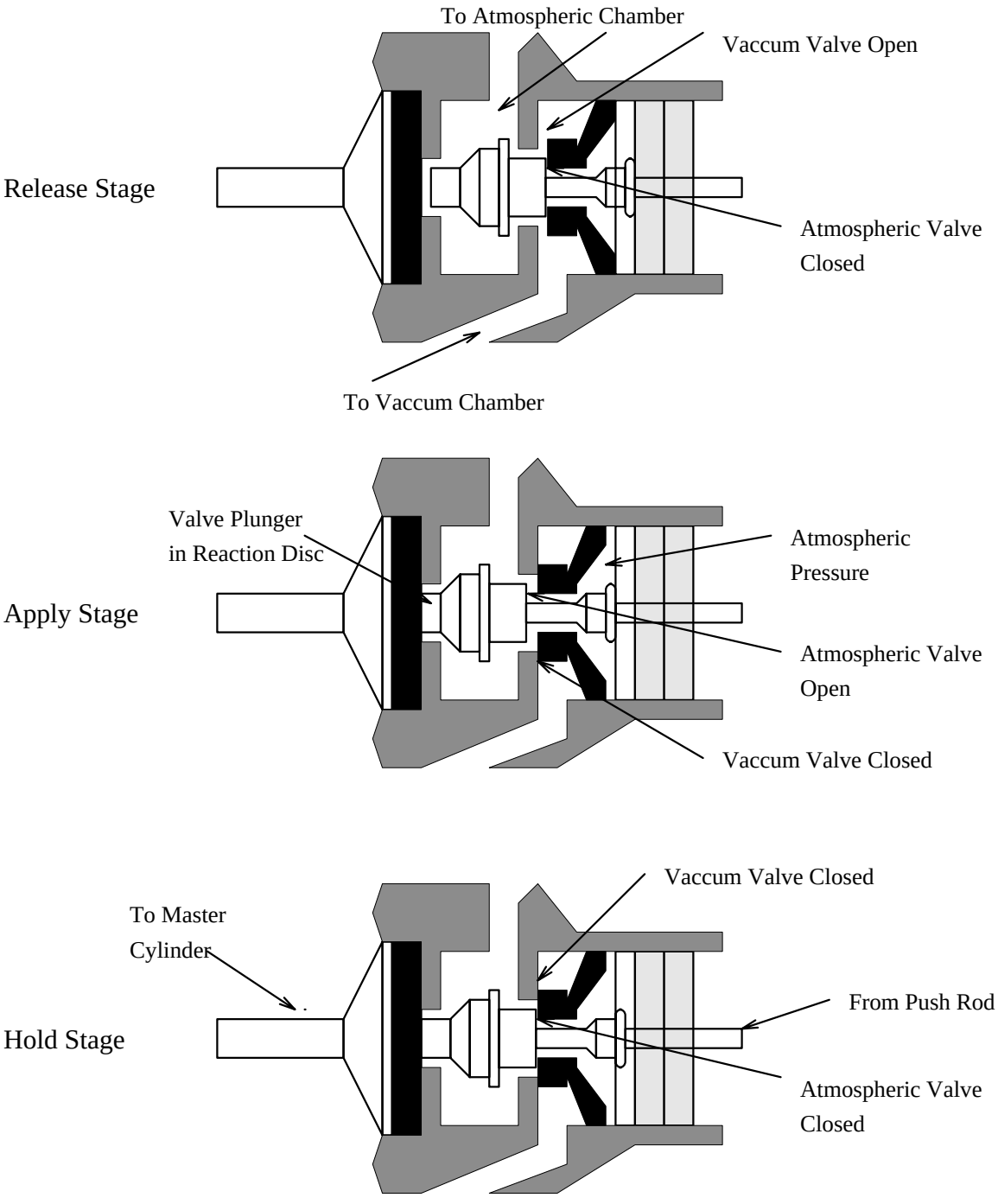

Figure 4: Vacuum Booster Operation

2.3 Master Cylinder

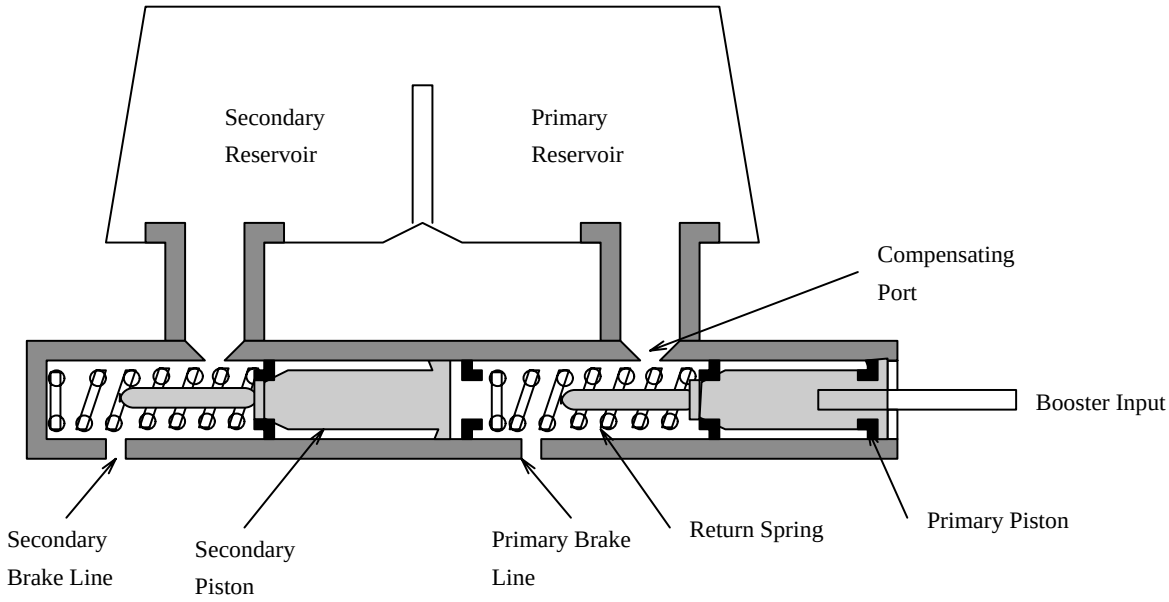

Figure 5: Block Diagram of Master Cylinder

The block diagram of a tandem master cylinder is shown in Figure 5. The input force, after being amplified by the vacuum booster, is applied through a push rod to the primary piston. The secondary piston, however, is pushed by the hydraulic force built up by the primary piston.

Each portion of the master cylinder has its own separate reservoir, compensating port and outlet port. When an input force is large enough to move the primary piston to close the compensating port, pressure begins to build up between the primary and secondary piston. When the secondary compensating port is closed, pressure buildup occurs in the secondary portion too. At the same time hydraulic pressure developed during this operation is transferred through the primary and secondary brake lines to the brake pads.

As discussed in [6], since the masses of the pistons are negligible, the dynamics associated with them can be neglected.

3 Proposed Brake Model

A series of experiments are conducted on the test bench of the brake subsystem. Some of the results of the experiments with step inputs of different magnitudes (corresponding to inputs of different duty cycle) are shown in Figures 6 and 7. These figures portray two basic modes of operation of the system: building and bleeding pressure modes. Another

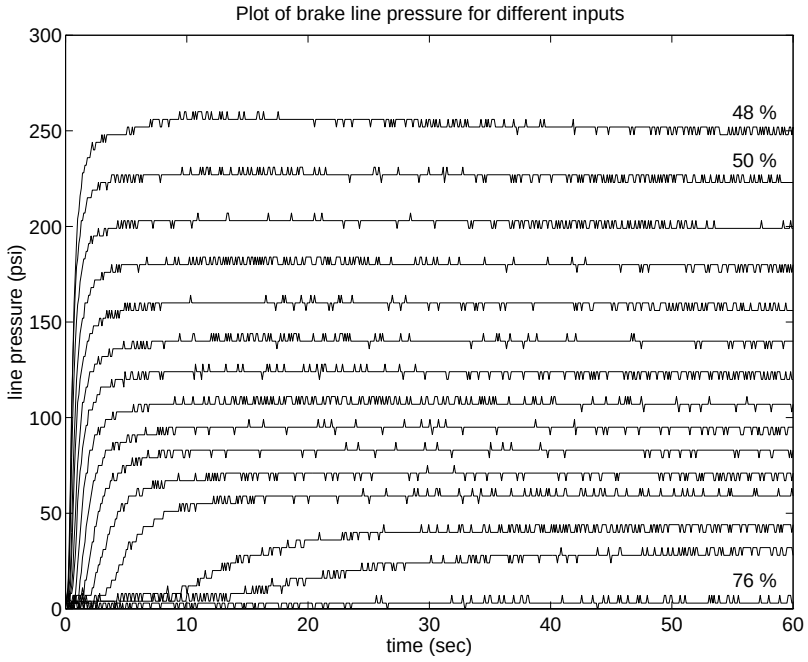

Figure 6: Brake line pressure for building mode. Inputs range from duty cycle of 76 to 48 %

important system feature, which can be observed from these figures, is the variable time delay associated with different inputs and operating modes.

Since, the time delay is an important factor in braking operations, a special attention was given to it in this study. A large time delay of the order of 0.2 second is observed for the relaxed system, i.e., when the line pressure is zero. This time delay becomes negligibly small ($\approx 0.01sec$) for any line pressure other than zero. Hence this leads to the following theoretical relation:

$$t_d = \begin{cases} 0.2 & \text{if } x = 0 \\ 0.01 & \text{if } x > 0 \end{cases} \tag{1}$$

where t_d and x denote the delay time and brake line pressure respectively. The system response in Figure 8 shows the time delays for the two cases discussed above.

The experimental results shown in Figure 6 and 7 suggest the presence of dominant first order dynamics. These results together with intuition motivate the following nonlinear dynamic model:

$$\dot{x}(t) = f_1(x(t), u(t^*), u(t^* - T)) \tag{2}$$

The variables in (2) are:

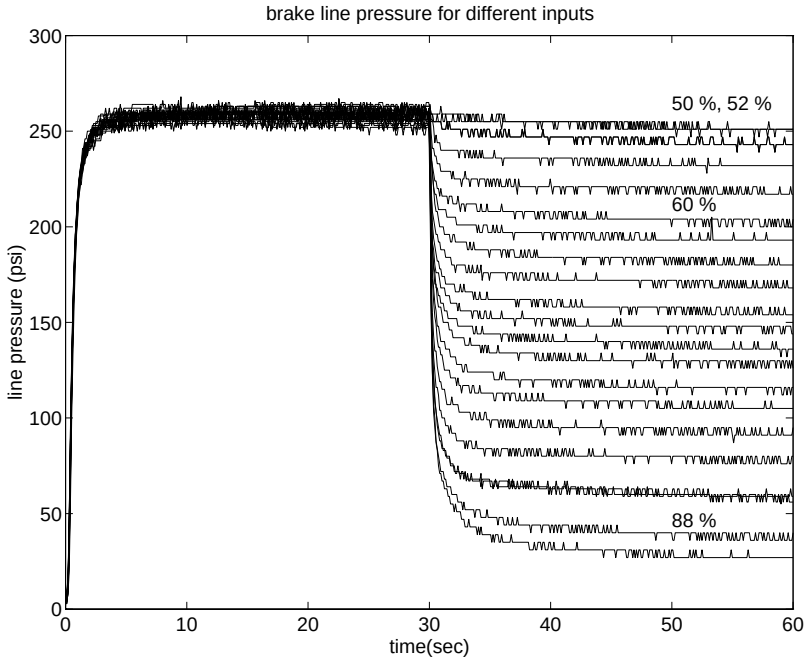

Figure 7: Brake line pressure for bleeding mode. The input is equal to 48 % for $0 \leq t < 30sec$ and is changed at $t = 30sec$ to different duty cycle values ranging from 50 to 90%.

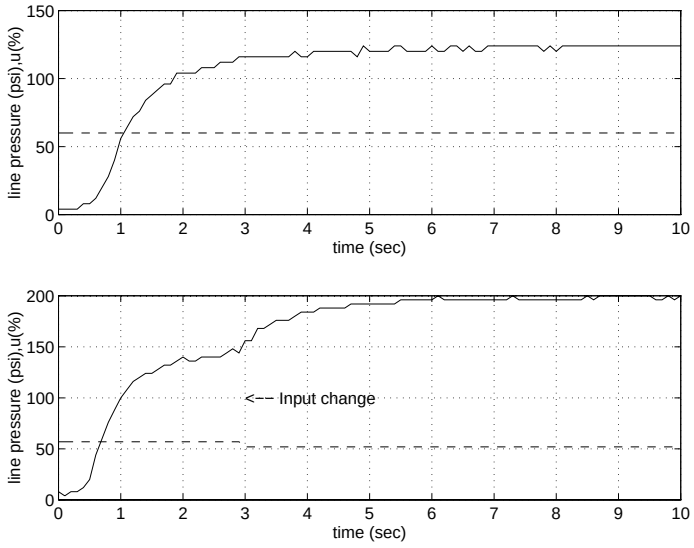

Figure 8: Top portion of the Figure shows that for the relaxed system a large time delay, 0.2 sec, is observed. However, for any subsequent changes in the input(bottom portion), the time delay is very small (≈ 0.01 sec).

x : system state (brake line pressure)

u : system input (duty cycle of the PWM signal)

f_1 : unknown function to be identified

where $x, u \in \mathcal{R}^1$, $t^* = t - t_d$, t_d is the time delay defined in (1), T is some small number (taken to be equal to the sampling period) and $u(t^* - T)$ denotes the previous input. As given in (1), the value of t_d is negligibly small except when the system is relaxed. Hence t_d can be safely assumed to be zero in (2). Since, in this study we use the input-output data which is obtained at sampling instants only, instead of the continuous model in (2), we propose the discrete time model:

$$x(k+1) = f(x(k), u(k), u(k-1)) \tag{3}$$

where k denotes the number of the sample, i.e., the time $t = kT$. The shape of the response for each fixed input, shown in Figures 6 and 7, can be approximated by a first order system given as:

$$x(k+1) = x(k) \; + \; Tb(a - x(k)) \tag{4}$$

where $a, b \in \mathcal{R}^+$. The parameters a and b in (4) may be used to characterize the steady state value and the speed of transient response respectively, for a given input $u(k)$. These parameters are nonlinear functions of the input u and state x of the system. The experiments show that the steady state value of the pressure a can be modeled as:

$$a = g(x(k), u(k)) \tag{5}$$

The speed of transient response (time constant) b vary significantly for different initial conditions and is sensitive to the previous history of the system, i.e., depends not only on the current input $u(k)$, but also on the previous input $u(k-1)$. This phenomenon can be explained in terms of nonlinear fluid dynamics. The change in pressure is significantly slow if an input change occurs near a steady state pressure condition. Hence the system time constant represented by b depends on the current pressure relative to the steady state pressure for the previous input. This suggests a functional form for the parameter b, which is given as:

$$b = h(x(k), u(k), u(k-1)) \tag{6}$$

In (5) and (6), g and h are unknown functions to be identified.

4 Parameter Identification

The identification of the unknown parameters (functions) a, b was done in two steps.

Step 1: Fixed step inputs were used to identify the steady state value a and time constant $1/b$ for each input.

Step 2: A series of staircase signals are used to modify the results of step 1.

The motivation of breaking down the identification process into two steps follows from the fact that the system response shown in Figures 6 and 7, for a fixed input, can be approximated by the response of a linear system to a step input. Hence standard results from linear system identification can be used to estimate the parameters. In the step 2 the nonlinear behavior of these parameters is explored by using staircase signals. These signals cover the possible changes in the input that excite the building and bleeding modes of the system and enable us to study the switching process between these modes. The results from these experiments are used to modify the parameters a and b so that their values are valid for possible input variations applied to the system.

Finally it is shown that with these parameters, identified by using step and staircase signals, a fairly accurate matching between the model and the actual system can be achieved for continuously varying inputs. This is due to the fact that any continuous signal can be approximated by a staircase signal, where the accuracy of the approximation depends on the chosen step size. This approximation can be represented as:

$$u(t) = u(kT) \qquad kT \leq t < (k+1)T \tag{7}$$

Where T is the sampling time and should be sufficiently small compared with the bandwidth of the input signal $u(t)$ and system dynamics.

4.1 Step Inputs

The step response curves shown in Figures 6 and 7 for each fixed input u can be approximated as a solution to the first order linear differential equation, discretized at time step kT, i.e.,

$$x(k) = x(0)(1 - Tb)^k \; + \; a(1 - (1 - Tb)^k) \tag{8}$$

where

a : steady state value

$1/b$: time constant

$x(0)$: initial condition

This simplification helps us to identify the parameters a and b for each input separately, by using standard curve fitting techniques. It should be noted that the approximation given in (8) which uses a single exponential function does not accurately describe the system response for inputs with duty cycle greater than 68 % in low pressure region. Hence the deviation between the predicted system response using the model and actual system is large for small line pressures. However, line pressures below 60 psi, corresponding to the aforementioned inputs, have little or no significance in actual braking. Hence this approximation has no effect on model accuracy within the range of line pressures of interest.

The steady state value of the line pressure, a, in the building mode is found to be relatively insensitive to the state x of the system. Furthermore, the two modes of operation shown in Figures 6 and 7 have different steady state values and slopes for the same inputs. The reason is the hysteresis produced due to friction, pre-loaded spring inside the vacuum booster and dead zone associated with the master cylinder and booster. Hence separate mappings for the two modes are required. The experimental results in Figure 6 suggest that for the building mode both a and b depend only on the current input, i.e.,

$$a = g(u(k)) \; ; \; b = h(u(k)) \qquad \text{(building)} \tag{9}$$

On the other hand for the bleeding mode a is a function of the current input whereas b depends also on the current state x, i.e.,

$$a = g^*(u(k)) \; ; \; b = h^*(u(k), x(k)) \qquad \text{(bleeding)} \tag{10}$$

These mappings g, h, g^* and h^* are given in Tables 3 and 4 respectively.

4.2 Staircase Inputs

Another series of experiments was conducted with inputs changing from one value to a different value and these changes were made to occur at different line pressures. Results show that the values of a calculated in these cases are consistent with those given in Table 3. The values of b, however, vary significantly and are found to be a function of the current pressure, x, at which the input was changed. Experiments show that the change in the value of b is noticeable if the input is changed at a pressure which is more than 50% of the steady state value of the previous input. This change shows a monotonically decreasing behavior, with a maximum reduction of around 25% at a pressure approximately equal to the steady state value. The change in the value of b as a function of the current line pressure for two different Δu is shown in Figure 9. Guided by the experimental results, the following linear approximation was introduced to model this change:

$$b = h(u(k)) \left(\frac{5}{4} - \frac{x(k)}{2g(u(k-1))} \right) \text{ when } x(k) \geq \tfrac{g(u(k-1))}{2} \tag{11}$$

The experimental results also indicate that the change in b occurs only if the input changes, since b corresponds to the dynamics associated with the system which do not

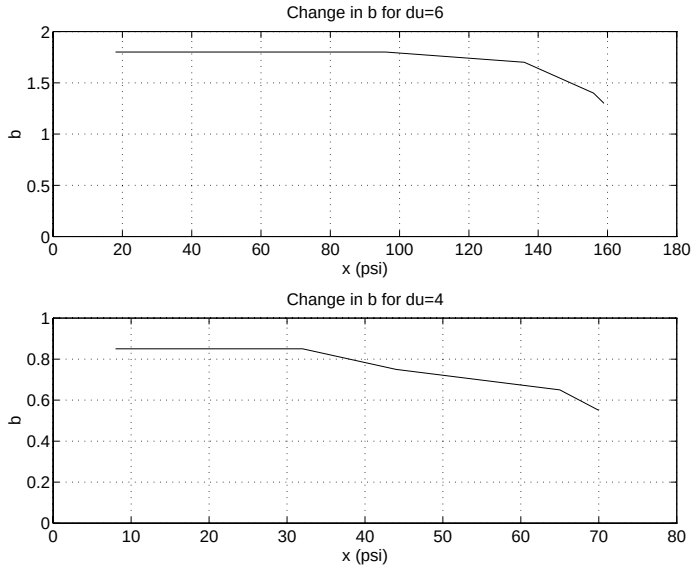

Figure 9: Change in b for change in input from 56% to 50% ($\Delta u = 6$) and from 68% to 64% ($\Delta u = 4$)

significantly change for a constant input. Whereas, the relation given in (11) updates the value of b at each sampling instant, which can be handled by introducing b as a state of the system as follows:

$$b(k+1) = \begin{cases} b(k) & \text{if } \Delta u = 0 \\ p_b b(k) \ + \ z_b \xi(k) & \text{else} \end{cases} \tag{12}$$

$$\xi(k) = \begin{cases} h(u(k)) & \text{if } x(k) < \frac{g(u(k-1))}{2} \\ h(u(k)) \left(\frac{5}{4} - \frac{x(k)}{2g(u(k-1))} \right) & \text{if } x(k) \geq \frac{g(u(k-1))}{2} \end{cases} \tag{13}$$

Where $\Delta u = u(k) - u(k-1)$, p_b and z_b are design parameters to smooth out the effects of switching, which is justifiable since the system dynamics do not show sudden changes. As explained later, this filtering would also help in the control design.

From Table 3, it is obvious that due to hysteresis, $g^*(u(k)) \geq g(u(k))$. From the experiments it was found that if a change in the input causes the system state to be switched from building to bleeding mode with $g^*(u(k)) > g(u(k-1))$ then $a = x(k)$, and the line pressure x would maintain its previous value. Hence for the bleeding mode, a, in (10) can be rewritten as:

$$a = min(x(k), g^*(u(k))) \tag{14}$$

The condition for determining the current mode of operation is:

$$x < g(u(k)) \ \Rightarrow \text{pressure is building} \tag{15}$$

This means that if the current pressure is strictly less than the steady state value for the current input, then the system is in the building mode. On the other hand if the current pressure is greater than or equal to the steady state pressure for the current input, then the system is in the bleeding mode. Hence by using the condition (15) the results given in (10), (14), (12) and (13) can be combined to give the final form of the model as:

$$x(k+1) = x(k) \; + \; Tb(k)(a(k) - x(k)) \tag{16}$$

$$a(k) = \begin{cases} g(u(k)) & \text{if } x(k) < g(u(k)) \\ min(x(k), g^*(u(k))) & \text{if } x(k) \geq g(u(k)) \end{cases} \tag{17}$$

$$b(k+1) = \begin{cases} b(k) & \text{if } \Delta u = 0 \\ p_b b(k) \; + \; z_b \xi(k) & \text{else} \end{cases} \tag{18}$$

$$\xi(k) = \begin{cases} h(u(k)) & \text{if } x(k) < \frac{g(u(k-1))}{2} \\ h(u(k)) \left(\frac{5}{4} - \frac{x(k)}{2g(u(k-1))} \right) & \text{if } x(k) \geq \frac{g(u(k-1))}{2} \\ h^*(u(k), x(k)) & \text{if } x(k) \geq g(u(k)) \end{cases} \tag{19}$$

The model described by (16)-(19) was simulated for different inputs and its response compared with that of the actual system. The results are shown in Figures 14 and 15. From Figure 15, we see that the actual system and model output differ for low pressure values (≤ 60 psi). However, as discussed before, due to the less significant effects of these pressure values on actual braking, this error is not severe.

It can also be seen form Figure 15 that for pressure values greater than 60 psi the error is within ± 8 psi. These error values are not large considering the fact that the pressure sensor used in the actual system has resolution of 4 psi. Furthermore, from Figure 15 it is obvious that the model output for staircase approximation of continuous signals is the same as that of the original signal. Hence, the estimates of the parameters a and b which were calculated as though the input signal is made up of finite steps hold even when the step width T is reduced to zero.

The limitations of the model (16)-(19) are the following:

1. The model accuracy depends mainly on the accuracy of identification of the parameters a and b.
2. The modification for b given by (11) holds only if $x < g(u(k-1))$, i.e., steady state is not attained. When steady state is actually achieved, the value of b shows a further decrease as time increases. In other words, the longer the system stays at one steady state value, the harder it is for the system to change the state. It was found by experiments that for a fixed input the steady state is not attained for a step width of less than 5 seconds, hence in this case the approximation given by (11) holds true. This is not a severe limitation considering the fact that actual braking commands do fall into this category.

5 Control Design

The nonlinearity of the model of the brake subsystem under consideration is in the form of a hysteresis and variable time delay. The main objective of the controller design in this paper is to make the performance of the brake subsystem as uniform and robust as possible throughout the range of operation. One way to achieve this objective is to use feedback linearization to cancel the nonlinearities of the system.

The design of the brake controller in this paper follows the guidelines provided by the feedback linearization techniques given in [12]. The brake model given in (16) has no explicit control input term. Since the parameter a in the brake model is a nonlinear function of the control input u and state x and the inverse mapping

$$u(k) = g^{-1}(a(k), x(k)) \tag{20}$$

is guaranteed to exist for all values of a and x within the operating range ($\mathcal{S}_o$,$\mathcal{U}_o$) of the system, where,

$$\begin{aligned} &\mathcal{S}_o = \{y \in \mathcal{R} : \ |y| \ \leq P_{max}\} \qquad \mathcal{U}_0 = \{u \in \mathcal{R} : \ u_{min} \leq u \leq u_{max}\} \\ &\forall a, x \in \mathcal{S}_o \quad \Rightarrow \quad g^{-1} \ exists \ and \ u \in \mathcal{U}_o \end{aligned} \tag{21}$$

where P_{max} is the maximum allowable pressure, u_{min} and u_{max} represent the minimum and the maximum allowable control input respectively. Hence with the condition given in (21), we can consider a to be the virtual control input. This assumption would help us to linearize the system by using standard input-output feedback linearization techniques. The controller design proceeds by first linearizing the brake model (16), with output $x(k)$ and input a, without changing the internal state dynamics $b(k)$ given in (18).

We first let

$$a(k) = \frac{1}{Tb(k)}(\alpha x(k) + \omega(k)) \ + \ \left(1 - \frac{1}{Tb(k)}\right) x(k) \tag{22}$$

where α is some design constant and ω is the new input. The resulting system is:

$$x(k+1) = \alpha x(k) \ + \ \omega(k) \tag{23}$$

Since a is given by (22) for some constant α and ω is a signal to be computed, the control input u can be calculated using the inverse mapping (20). The feedback linearized system is given by (23), whose transfer function is:

$$G'(z) = \frac{x(z)}{\omega(z)} = \frac{1}{z - \alpha} \tag{24}$$

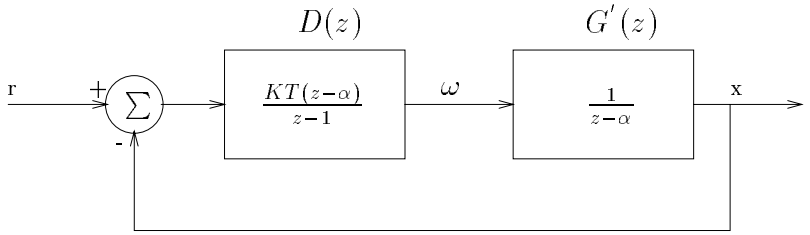

Figure 10: Block diagram of the closed loop system.

The input ω can now be selected to meet the control objective for the feedback linearized system (23). In general ω could be of the form:

$$\omega = D(z)(r - x)$$

as shown in Figure 10, where $D(z)$ will be chosen to meet the control objective. For example, for:

$$D(z) = K_P + \frac{K_I T}{z-1} = \frac{K_P(z-1) + K_I T}{z-1} \tag{25}$$

we have a PI compensator whose parameters K_P, K_I can be chosen for stability and zero steady state error. The loop transfer function with the addition of the PI compensator becomes:

$$L(z) = K_P \frac{(z-1) + \frac{K_I T}{K_P}}{(z-1)(z-\alpha)} \tag{26}$$

Hence with the addition of a PI compensator the order of the closed loop system has increased. This, however, can be avoided by carefully selecting the gains K_P and K_I. One such combination is given by:

$$K_P = KT \qquad K_I = K(1-\alpha)$$

where $K > 0$ is a design constant to place the closed loop pole at a desired location. Hence the input ω in (23) becomes:

$$\omega = \frac{KT(z-\alpha)}{z-1}(r - x) \tag{27}$$

The closed loop transfer function $T(s)$ shown in Figure 10 is given by:

$$T(z) = \frac{x(z)}{r(z)} = \frac{KT}{z - 1 + KT} \tag{28}$$

The control law is summarized in Table 1 and is represented by the block diagram shown in Figure 11.

$$\omega(k) = \frac{KT(z-\alpha)}{z-1}(r(k) - x(k))$$

$$a(k) = \frac{1}{Tb(k)}(\alpha x(k) + \omega(k)) \; + \; \left(1 - \frac{1}{Tb(k)}\right) x(k)$$

$$u(k) = g^{-1}(a(k), x(k))$$

Table 1: Summary of Control Law

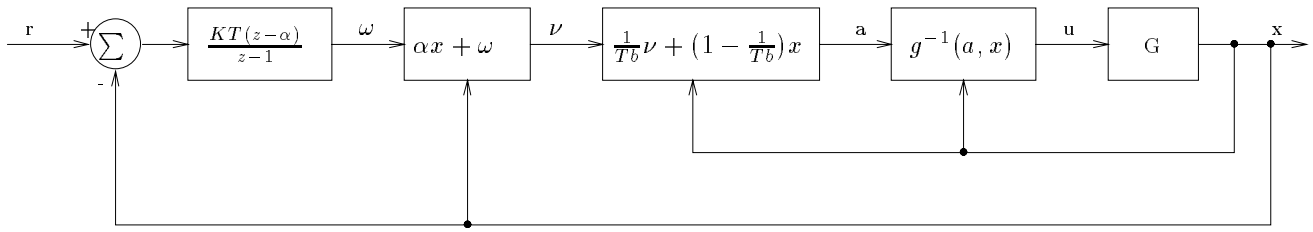

Figure 11: Block diagram for implementation of the feedback linearized control system.

5.1 Controller Modifications

The control input generated by the feedback linearization shown in Table 1 is calculated based on the assumption that there is no saturation of the control input. However, from the safety point of view a limited control authority is available in the given system. Hence to avoid performance deterioration, some additional logic is embedded within the standard PI compensator. These modifications along with some justification are presented below:

• In order to avoid the integration wind up problems a limited integrator is used in place of the ideal integrator.

• In order to avoid overshoot while maintaining swiftness of response, the logic shown in Figure 12 is added to the PI compensator. Since the brake subsystem under consideration has a large delay, $\approx 0.2sec.$ at start up, the branch labeled *delay kill* in Figure 12 stops integrator accumulation during this interval. This reduces the saturation of the control input during the delay period and helps to avoid overshoot at low operating pressures.

• To reduce overshoot at high pressure, the branch labeled *shoot kill* cuts off integrator when either:
- the nonlinear function a, used as linearization input, exceeds the maximum steady state

pressure value and the actual pressure x is less than the desired one - or when a is negative and the brake pressure is greater than the desired. This modification results in minimum possible overshoot for normal and high pressure regions. Hence during initial startup time and at the time when the controller output is saturated, this logic avoids excessive integrator accumulation, that may cause subsequent overshoots. The output of the PI compensator is now given as:

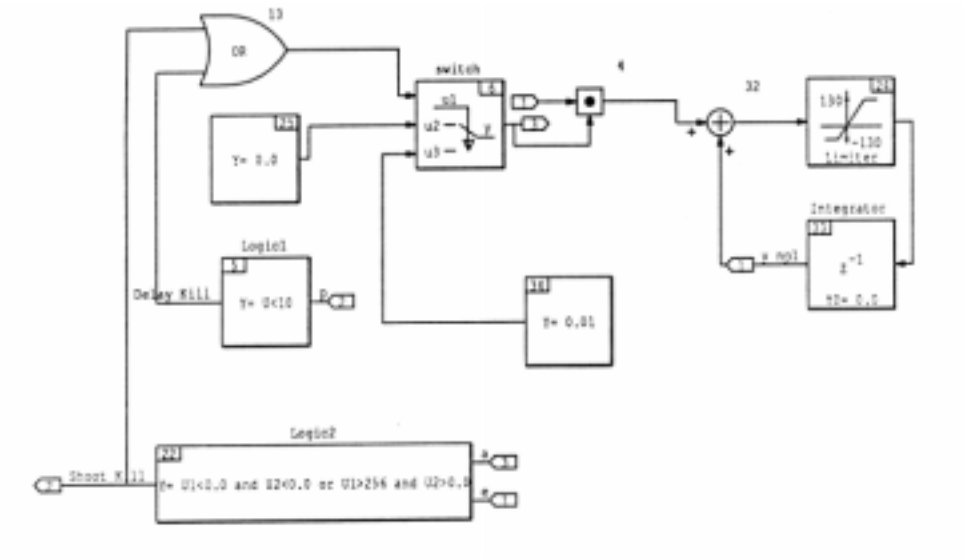

Figure 12: Block diagram of the modified integrator.

$$\omega(k) = \begin{cases} KT(r(k) - x(k)) & \text{if } x(k) < P_{min} \text{ or } ((r(k) - x(k)) < 0 \text{ and } a(k) < 0) \\ & \text{or } (a(k) > a_{max} \text{ and } (r(k) - x(k)) > 0) \\ \frac{KT(z-\alpha)}{z-1}(r(k) - x(k)) & \text{else} \end{cases} \quad (29)$$

where P_{min} is the minimum line pressure in idle state, when the time delay is large. Since the inverse mapping, $u = g^{-1}(a, x)$, is guaranteed to exist when the inputs a, x are within the physical constraints imposed by the equipment, a saturation function $p(.)$ is introduced at the output of a.

$$p(a(k)) = \begin{cases} a(k) & \text{if } a_{min} < a(k) < a_{max} \\ a_{min} & \text{if } a(k) < a_{min} \\ a_{max} & \text{else} \end{cases} \quad (30)$$

where $a_{min} = 0$ and $a_{max} = P_{max}$, P_{max} is the maximum allowable pressure. Some simulation results before and after addition of this logic are shown in Figure 16. A comparison

of the attainable performance using this modification, with the standard PI compensator is given in Table 2.

controller	*rise time*	*settling time*	*s.s. error*	*overshoot*
Standard PI	1.0 sec	3.5 sec	≈ 0	10 %
Modified PI	1.1 sec	2.5 sec	≈ 0	0

Table 2: Comparison of performance

With the proposed modification, the main characteristics of the closed loop system are summarized as follows:

- The step response is fast enough to meet the AVCS performance specifications [2]
- There is no overshoot or undershoot.
- The steady state error for step inputs is equal to zero.

6 Stability Analysis

We first discuss the stability properties of the open loop system. The nonlinear functions $a = g(x, u)$ and $b = h(x, u)$ in (17) and (18) are guaranteed to be bounded, i.e.,

$$g(x, u) \in \mathcal{C}_1 = \{y_1 \in \mathcal{R} : a_{min} \leq y_1 \leq a_{max}\} \tag{31}$$

$$h(x, u) \in \mathcal{C}_2 = \{y_2 \in \mathcal{R} : b_{min} \leq y_1 \leq b_{max}\} \quad \forall u, x(0) \in \mathcal{L}_\infty \tag{32}$$

where $a_{min} \geq 0$ and $b_{min} > 0$. Hence for any bounded initial condition, any bounded input to the system would result in a bounded state, i.e.,

$$u, x(0) \in \mathcal{L}_\infty \Rightarrow x \in \mathcal{L}_\infty \quad \forall t \geq 0$$

Furthermore, $u \in \mathcal{U}_o \Rightarrow x \in \mathcal{S}_o$, where $\mathcal{U}_o$ and $\mathcal{S}_o$ are as defined in (21). As discussed before, the nonlinear function a is used in place of the control input u for linearization of open loop plant (16). As given by condition (21), if we guarantee that $a, x \in \mathcal{S}_o$ then it implies that $u \in \mathcal{L}_\infty$, rather $u \in \mathcal{U}_o$, where $\mathcal{U}_o$ forms the set of acceptable inputs to the system.

Theorem 1 *If the controller given in Table 1 with the modification (29) is initialized such that $u(k_0) \in \mathcal{U}_o$, then the closed loop signals ω, ν, a, u and x are bounded and $u \in \mathcal{U}_o$, $x \in \mathcal{S}_o$ $\forall k \geq k_0$.*

Proof: The assumption that at $t = k_0T$, $u \in \mathcal{U}_o$ is not restrictive as the controller would be initialized with some acceptable input. To establish the boundedness of all the signals in closed loop, we begin as follows:

We have that $u(k_0) \in \mathcal{U}_o \Rightarrow x(k_0) \in \mathcal{S}_o$. Considering the PI compensator, we can write:

$$\omega(k) = W(z)(r(k) - x(k)) \tag{33}$$

$$\Rightarrow \|\omega\|_2 \leq \|W(z)\|_\infty \|r - x\|_2 \tag{34}$$

where $r(k)$ is the desired output trajectory, obviously $r(k) \in \mathcal{S}_o, \Rightarrow (r(k_0) - x(k_0)) \in \mathcal{O}(\mathcal{S}_o)^*$. Since $W(z)$ is a stable proper transfer function, hence for $(r(k_0) - x(k_0)) \in \mathcal{O}(\mathcal{S}_o) \cap \mathcal{L}_2$, we have $\omega(k_0) \in \mathcal{O}(\mathcal{S}_o) \cap \mathcal{L}_2$. Denoting $\alpha x(k) + \omega(k)$ in (22) by $\nu(k)$, we have:

$$\|\nu(k_0)\|_2 \leq |\alpha| \, \|x(k_0)\|_2 \; + \; \|\omega(k_0)\|_2 \tag{35}$$

where α is a finite design constant chosen earlier, $\Rightarrow \nu(k_0) \in \mathcal{O}(\mathcal{S}_o) \cap \mathcal{L}_2$. Also from (22) we can write:

$$\|a(k_0)\|_2 \leq |c_1| \, \|\nu(k_0)\|_2 \; + \; |c_2| \, \|x(k_0)\|_2 \tag{36}$$

where $c_1 = \frac{1}{Tb(k_0)}$ and $c_2 = (1 - c_1)$ are finite constants as $b(k) \geq b_{min} > 0 \; \forall k$, $\Rightarrow a(k_0) \in \mathcal{O}(\mathcal{S}_o) \cap \mathcal{L}_2$. Finally the saturation function $p(.)$ defined in (30) ensures that $a(k_0) \in \mathcal{S}_o$.

Hence, from (21) we get $u(k_0 + 1) \in \mathcal{U}_o \Rightarrow x(k_0 + 1) \in \mathcal{S}_o$. Now by induction we can show that closed loop signals are bounded and $u(k) \in \mathcal{U}_o$, $x(k) \in \mathcal{S}_o$ for all $k \geq k_0$. □

7 Simulation and Implementation Results

The modified control law given in (29), (22), (30) and (20) is simulated using Matrixx and the nonlinear brake model. The block diagram of the closed loop system is shown in Figure 13. The simulation results of typical braking scenarios are shown in Figures 17a-19a. The simulation results confirm the claims made about performance in terms of zero steady state error, no overshoot and sufficiently fast response (limited by the equipment constraints).

The controller given in Figure 13 is also implemented on the actual brake system. The results obtained from the actual closed loop system are shown in Figures 17b-19b. The simulation results in Figures 17a-19a are almost identical to the actual closed loop system response shown in Figures 17b-19b. Furthermore, one of the design objectives to make the system behave linearly is proved by comparing the actual closed loop system response with that of the equivalent linear system ($\frac{KT}{z-1+KT}$). The comparison for the three inputs considered before is shown in Figure 21.

*A function $f(x)$ is $\mathcal{O}(x)$ if there exists a finite constant $c > 0$, such that $|f(x)| \leq c|x| \; \forall x$.

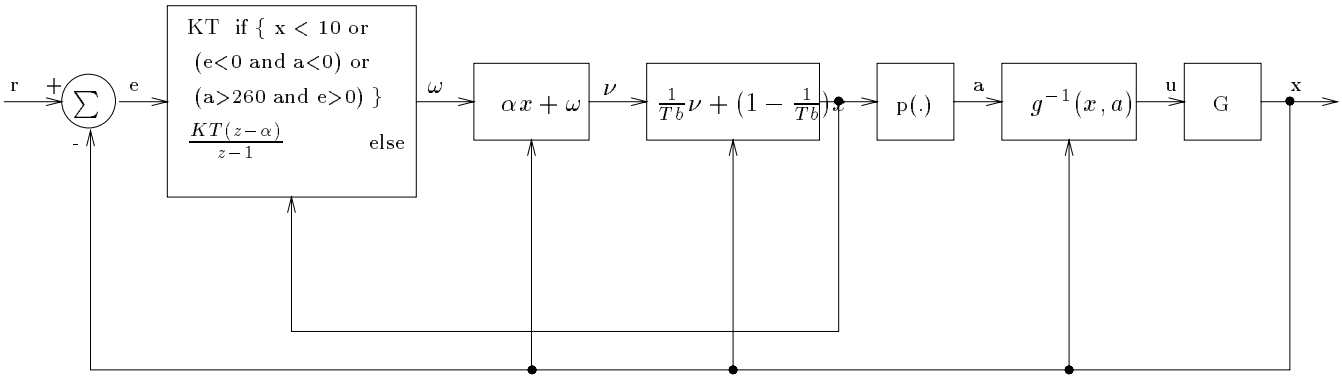

Figure 13: Block diagram of the feedback linearized control system.

8 Conclusion

A nonlinear model that describes the input output behavior of the brake subsystem of a Lincoln town car is developed. The model is simplified to resemble a first order linear system with nonlinear coefficients and time delays. The unknown parameters are identified by applying the standard curve fitting techniques to the data obtained by conducting experiments on the test bench. The hysteresis phenomenon is modeled by isolating the two operating modes, that is the building and bleeding modes, and identifying separate sets of parameters for each one. The worst case modeling error was found to be less than 5% within the range of interest.

A brake controller is developed using standard feedback linearization techniques on the nonlinear validated model. A PI compensator with intuitive modifications is introduced in the closed loop to meet the performance specifications. The controller has been shown to meet the possible performance requirements in an AVCS application by applying to the actual brake subsystem mounted on a bench.

Acknowledgment

We would like to thank Ford Motor Company for donating the brake test bench to us. We also like to thank Dr. Steve Eckert and Mr. Mark Peterson for helping us to set it up and for many useful technical informations and guidance.

References

[1] Shladover, S., E., "Longitudinal Control of Automotive Vehicles in Close-Formation Platoons", ASME Journal on Dynamic Systems, Measurement and Control, vol. 113, 1991, pp. 231-241.

[2] Shladover, S., E., Desor, C., A., Hedrick, J., K., Tomizuka, M., Warland, J., Zhang, W., B., McMohan, D., Peng, H., Sheikholselam, S., McKeown, N., "Automatic Vehicle Control Developments in PATH Program, IEEE Trans. on Vehicular Technology", vol. 40, 1991, pp. 114-130.

[3] Sheikholelslam, S., Desoer, C., A., "A System Level Study of the Longitudinal Control of a Platoon of Vehicles", ASME Journal of Dynamic Systems, Measurement, and Control, 1991.

[4] Varaiya, P., "Smart Cars on Smart Roads: Problems of Control", IEEE Transactions on Automatic Control, vol. AC-38, no.2, pp. 195-207, 1993.

[5] Chien, C., C., Ioannou, P., "Automatic Vehicle Following", Proc. American Control Conference, Chicago, Il., June 1992.

[6] Gerdes, J., C., Maciuca, D., B., Devlin, P., E., Hedrick, J., K., "Brake Modeling for IVHS Longitudinal Control", Winter Annual Meeting of the American Society of the Mechanical Engineers, 1993.

[7] Khan, Y., Kulkarni, P., and Youcef-Toumi, K., "Modeling, Experimentation and Simulation of a Brake Apply System", Proceedings of the 1992 American Control Conference, pp. 226-230.

[8] Nunney, M., J., "Light and Heavy Vehicle Technology", 2nd Edition, Newnes, Oxford OX2 8DP, 1992, pp. 516-552.

[9] Hedrick J. K., McMahon D., Narendran V., Swaroop D., "Longitudinal Vehicle Controller Design for IVHS System", Proceeding of American Control Conference", Vol. 3, pp. 3107-3112, June 1991.

[10] Xu Z., Ioannou P., "Throttle and Brake Control Systems for Automatic Vehicle Following", IVHS Journal, 1994, Vol. 1(4), pp.345-377.

[11] Hauksdottir A. S., Fenton R. E., "On the Design of Vehicle Longitudinal Controller", IEEE Transaction on Vehicular Technology, Vol. VT-34, No. 4, pp. 182-187, Nov. 1985.

[12] Slotine J. E., Li W., "Applied Nonlinear Control", Prentice Hall, Englewood Cliffs, NJ, 1991.

A Lookup Tables

u (%)	$a = g(u)$ (psi)	$b = h(u)$	$a = g^*(u)$ (psi)
48	253	1.8	253
50	226	1.7	253
52	202	1.6	252
54	181	1.4	251
56	159	1.2	245
58	140	1.0	233
60	124	0.9	219
62	108	0.75	194
64	94	0.65	182
66	83	0.50	170
68	70	0.35	157
70	60	0.20	148
72	48	0.1	138
74	30	0.1	129
76	5	0.1	116
78	0	0.1	107
80	0	0.1	94
82	0	0.1	79
84	0	0.1	65
86	0	0.1	57
88	0	0.1	40
90	0	0.1	29

Table 3: Least square fit values of functions g, h and g^* for the curves in Figures 6 and 7

u \ x	0	30	60	80	95	105	125	145	160	180	200	225	253
48	X	X	X	X	X	X	X	X	X	X	X	X	1.8
50	X	X	X	X	X	X	X	X	X	X	X	1.7	1.8
52	X	X	X	X	X	X	X	X	X	X	1.6	1.7	1.8
54	X	X	X	X	X	X	X	X	X	1.4	1.6	1.7	1.9
56	X	X	X	X	X	X	X	X	1.2	1.4	1.6	1.8	1.9
58	X	X	X	X	X	X	X	1.0	1.2	1.4	1.7	1.8	2.0
60	X	X	X	X	X	X	0.9	1.0	1.2	1.5	1.7	1.9	2.1
62	X	X	X	X	X	0.75	0.9	1.0	1.3	1.5	1.8	1.9	2.2
64	X	X	X	X	0.65	0.75	0.9	1.1	1.3	1.6	1.8	2.0	2.3
66	X	X	X	0.5	0.65	0.75	1.0	1.1	1.4	1.6	1.9	2.0	2.4
68	X	X	X	0.5	0.65	0.8	1.0	1.2	1.4	1.7	1.9	2.1	2.5
70	X	X	0.2	0.5	0.7	0.8	1.0	1.2	1.5	1.8	2.0	2.2	2.6
72	X	X	0.2	0.5	0.7	0.8	1.1	1.3	1.5	1.8	2.0	2.3	2.6
74	X	0.1	0.2	0.6	0.7	0.9	1.1	1.3	1.6	1.9	2.1	2.4	2.7
76	X	0.1	0.2	0.6	0.7	0.9	1.1	1.4	1.6	1.9	2.2	2.5	2.7
78	0.1	0.1	0.3	0.6	0.7	0.9	1.2	1.4	1.7	2.0	2.3	2.5	2.8
80	0.1	0.1	0.3	0.6	0.7	0.9	1.2	1.5	1.7	2.0	2.3	2.6	2.8
82	0.1	0.1	0.3	0.7	0.7	1.0	1.2	1.5	1.8	2.1	2.4	2.6	2.9
84	0.1	0.1	0.4	0.7	0.8	1.0	1.3	1.5	1.8	2.1	2.4	2.7	2.9
86	0.1	0.1	0.4	0.7	0.8	1.0	1.3	1.6	1.9	2.2	2.5	2.7	3.0
88	0.1	0.1	0.4	0.7	0.8	1.0	1.3	1.6	1.9	2.2	2.5	2.7	3.0
90	0.1	0.1	0.4	0.7	0.8	1.0	1.3	1.6	1.9	2.2	2.5	2.7	3.0

Table 4: Least square fit values of $b = h^*(u, x)$ for the curves in Figure 7. An X as a table entry indicates an invalid state for bleeding mode.

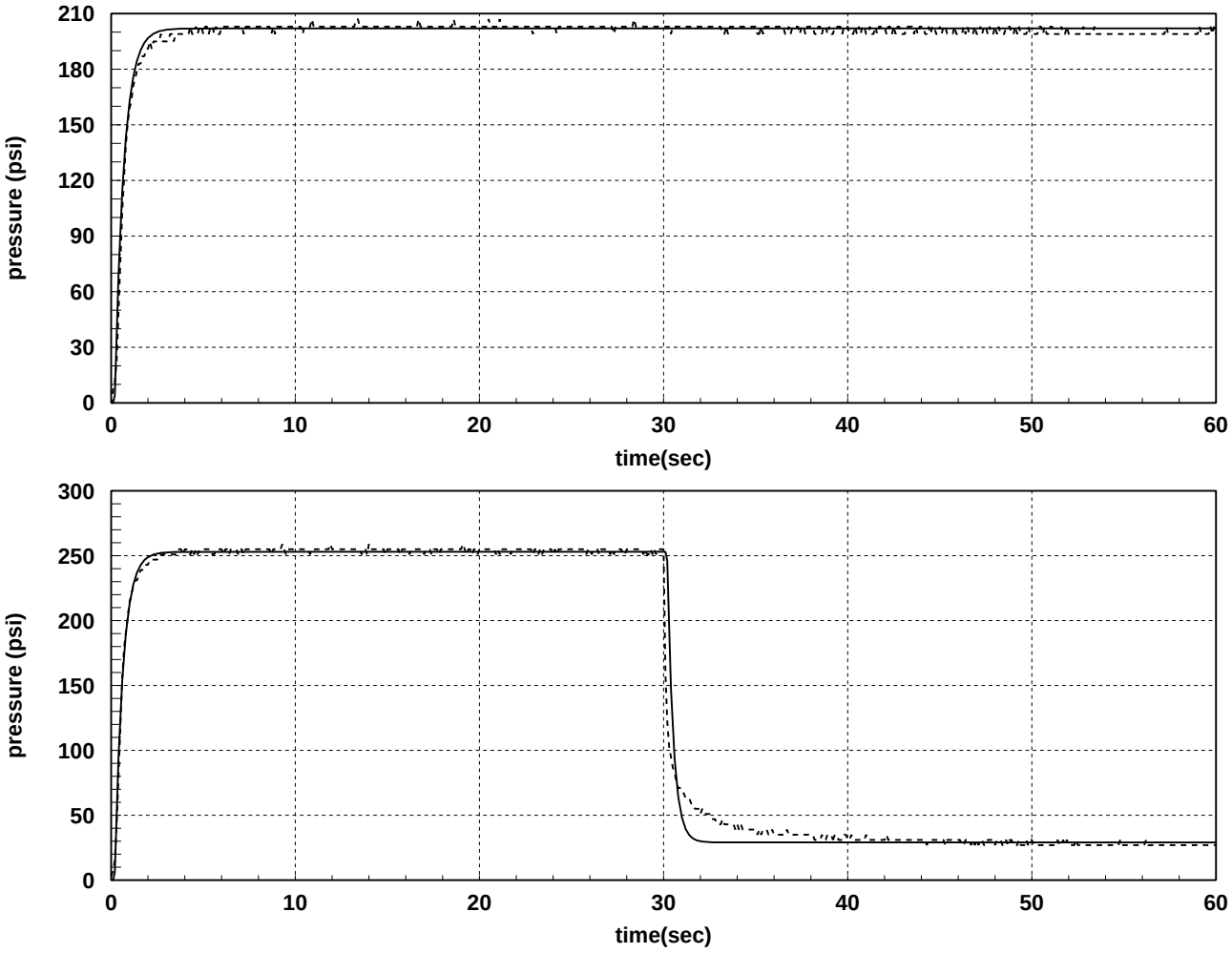

Figure 14: A comparison of the actual and model output for a step input of 52% is shown in the top portion of the Figure. Whereas in the bottom one input changes from 48% to 90% at t=30 sec.

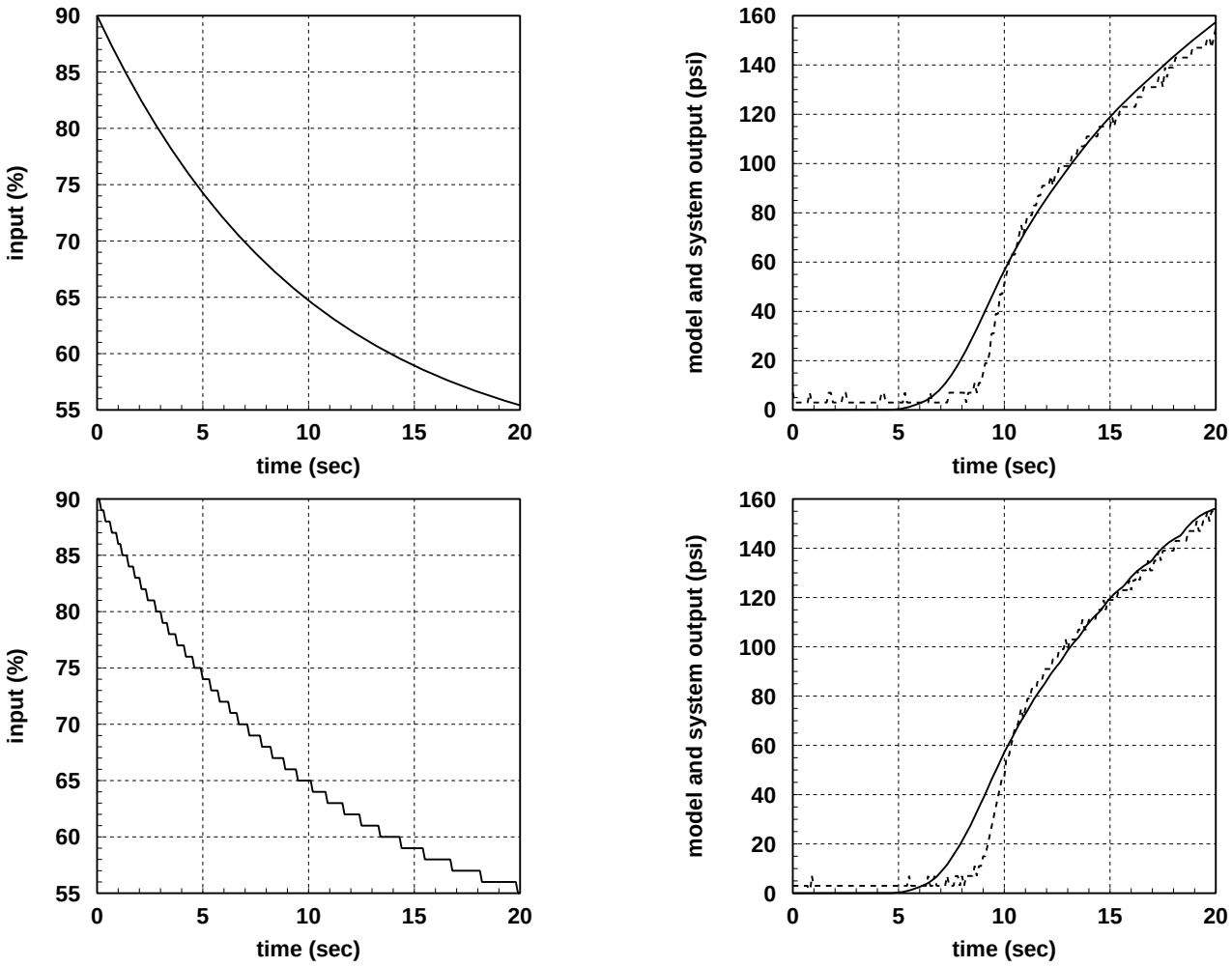

Figure 15: The top left portion of the Figure shows the input signal being applied to actual system and brake model for comparison. The system and model outputs are shown in top right position for given input signal. A staircase approximation of the same input signal is shown in bottom left graph. The comparison of outputs is shown in bottom right graph.

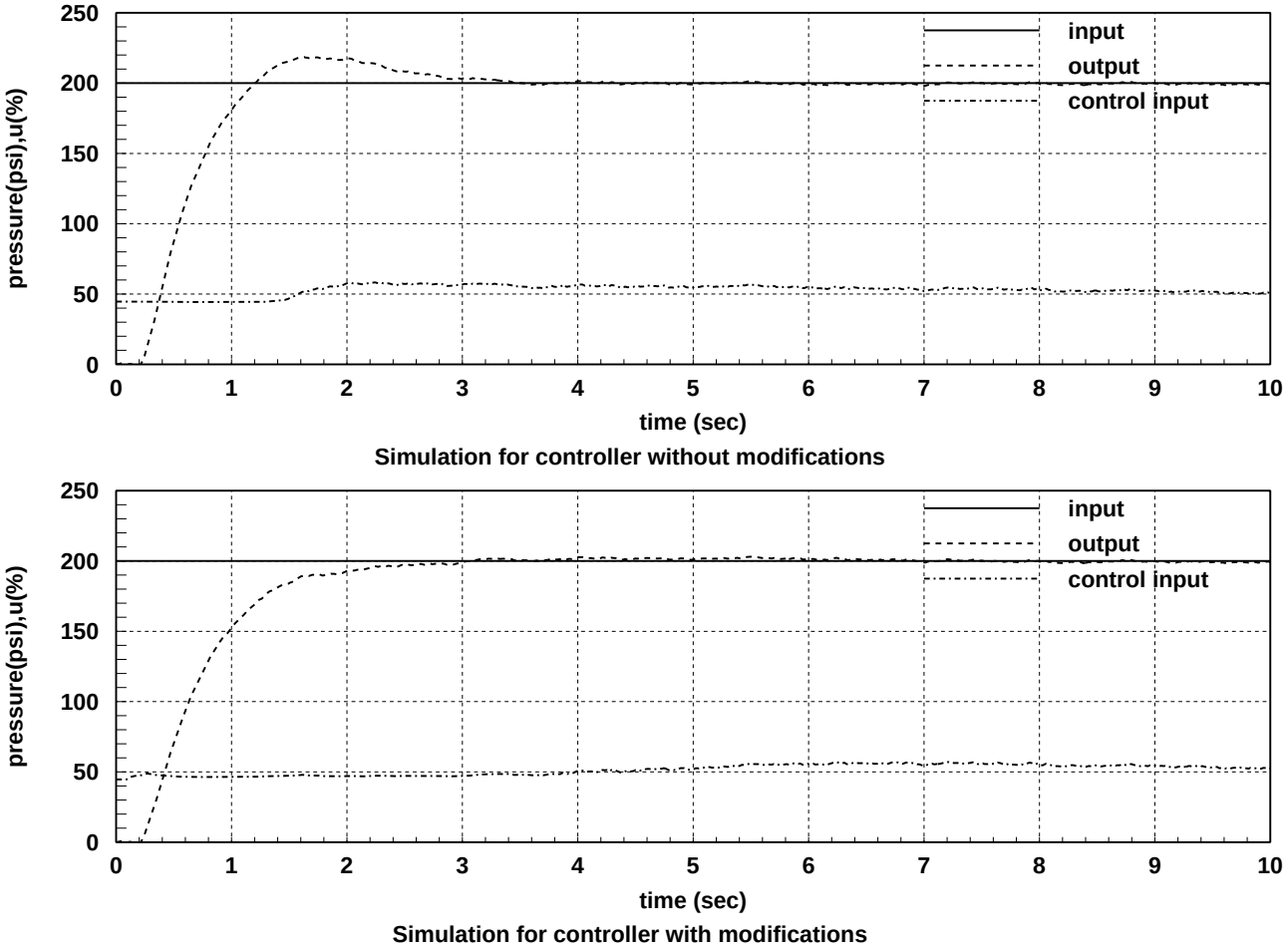

Figure 16: Comparison of closed loop response for PI compensator with and without modifications.

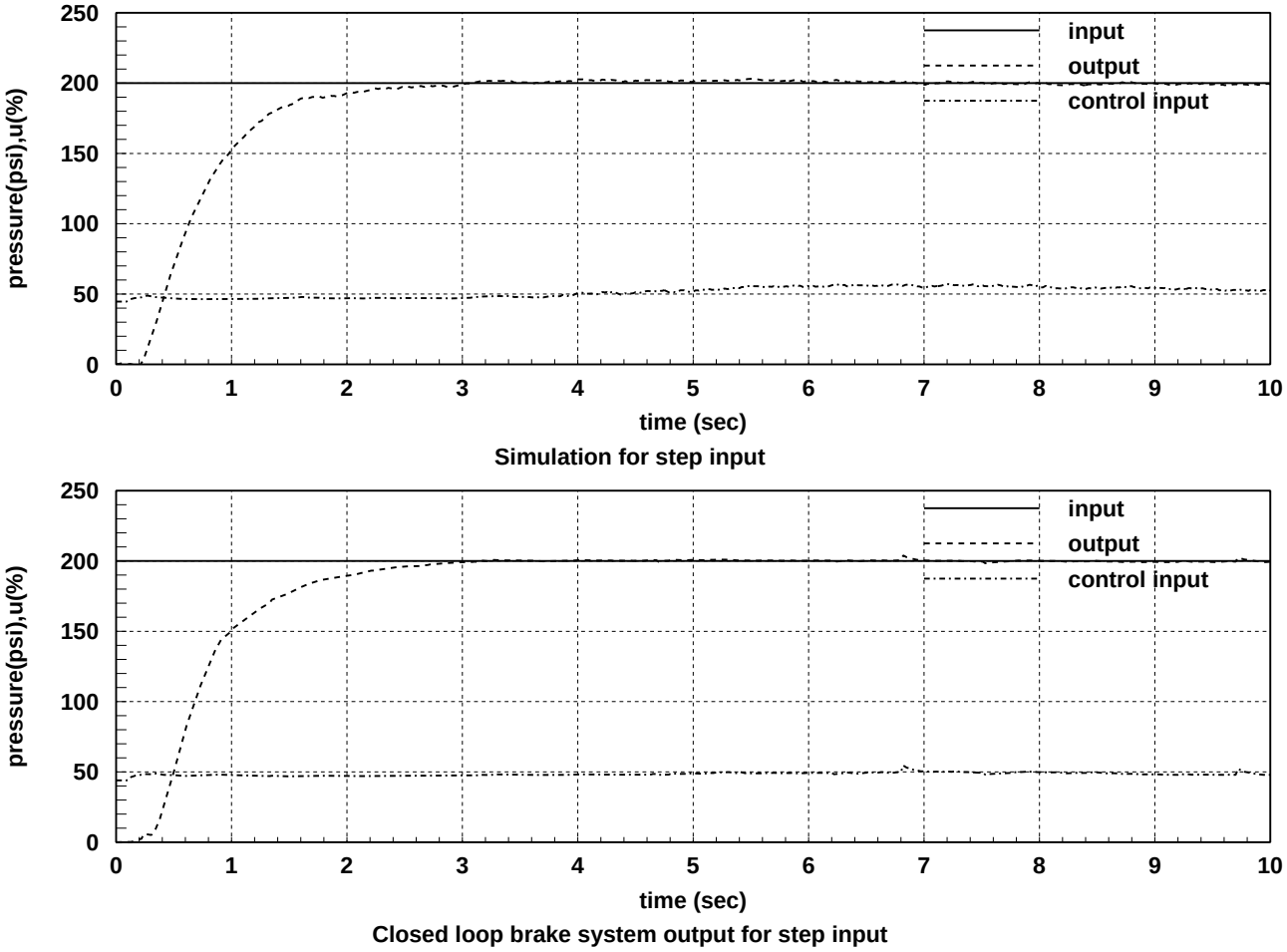

Figure 17: Simulation and actual system response for step input, corresponding to a desired pressure of 200 psi.

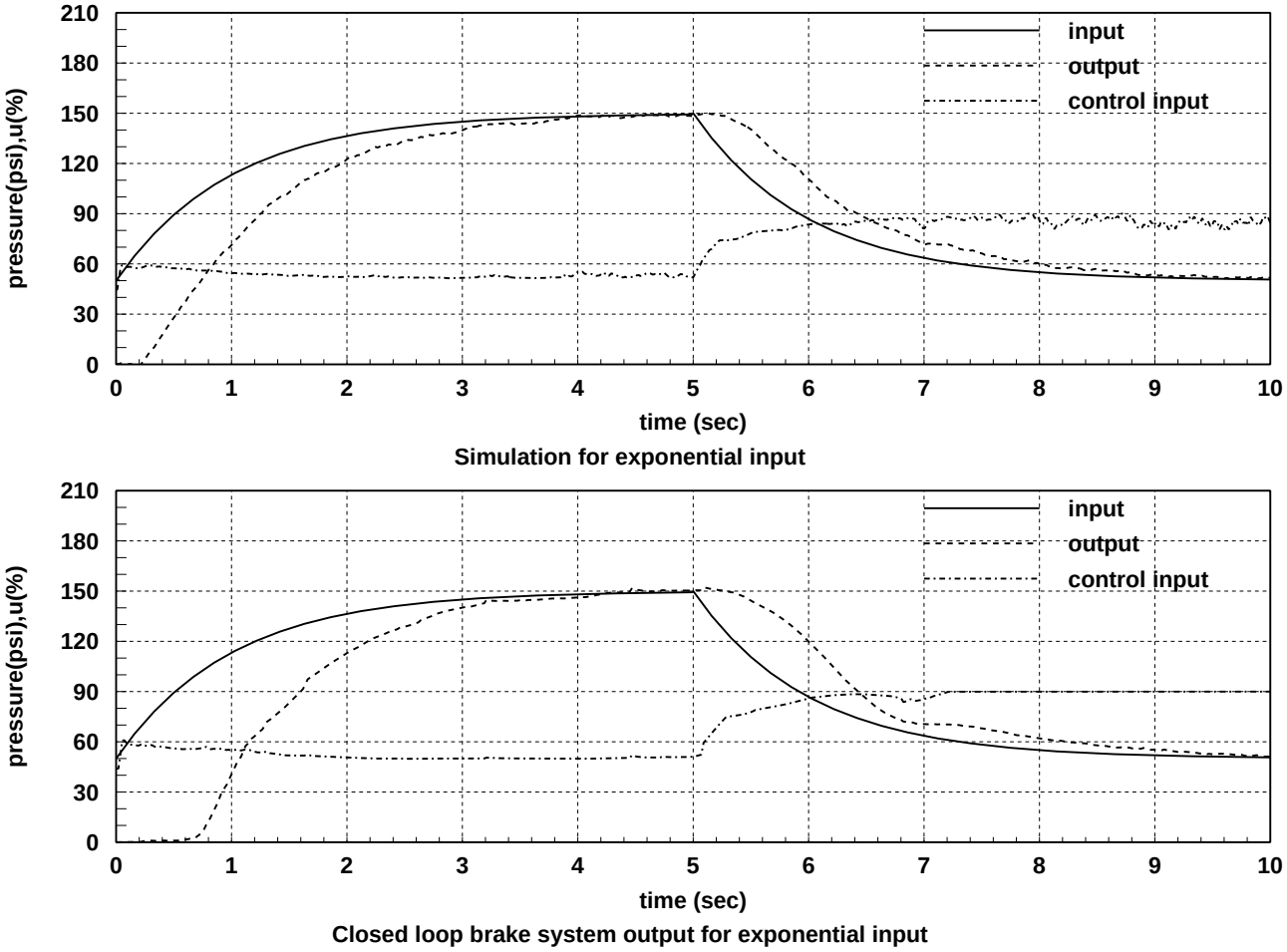

Figure 18: Simulation and actual system response for exponential input.

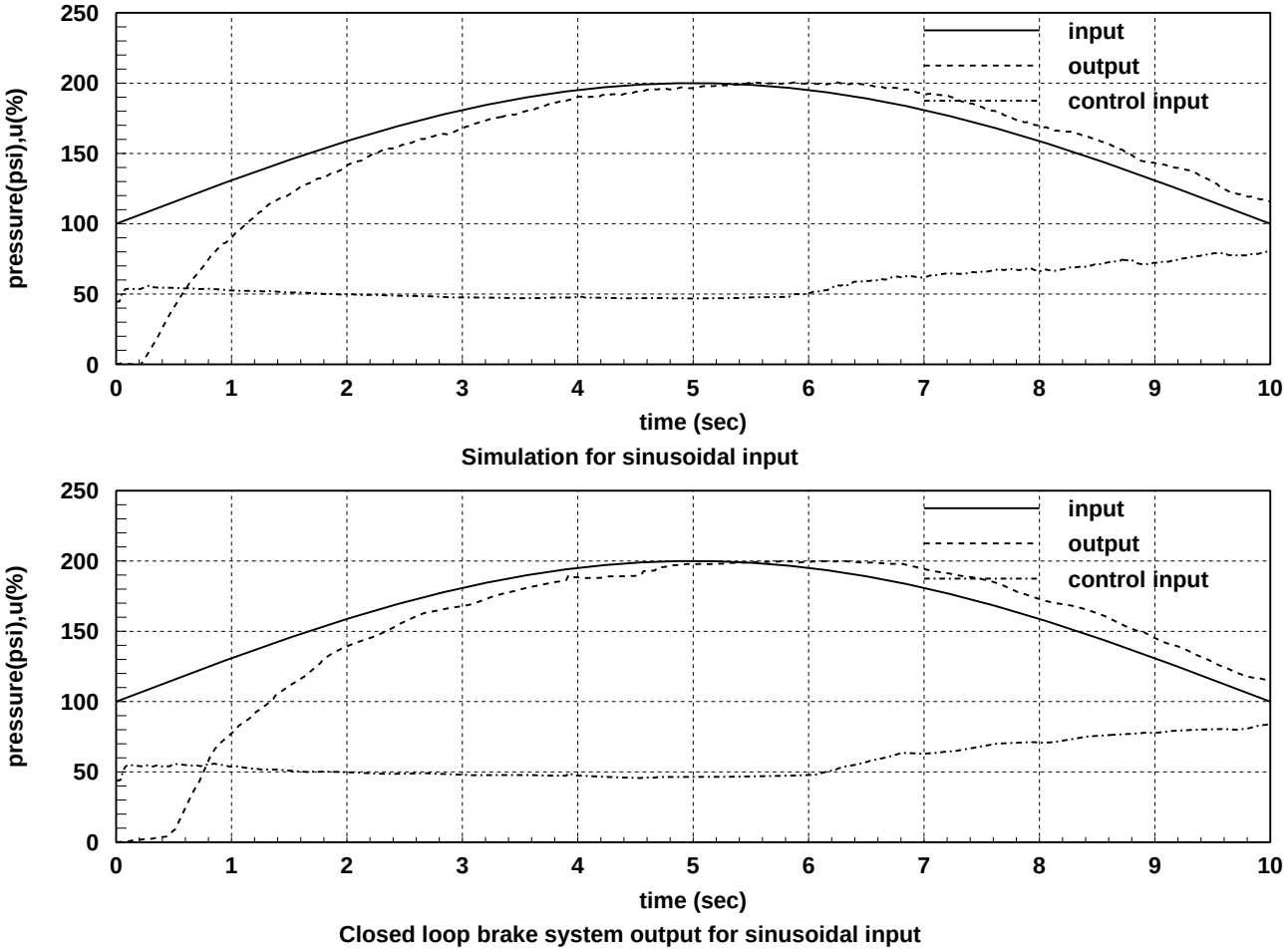

Figure 19: Simulation and actual system response for sinusoidal input.

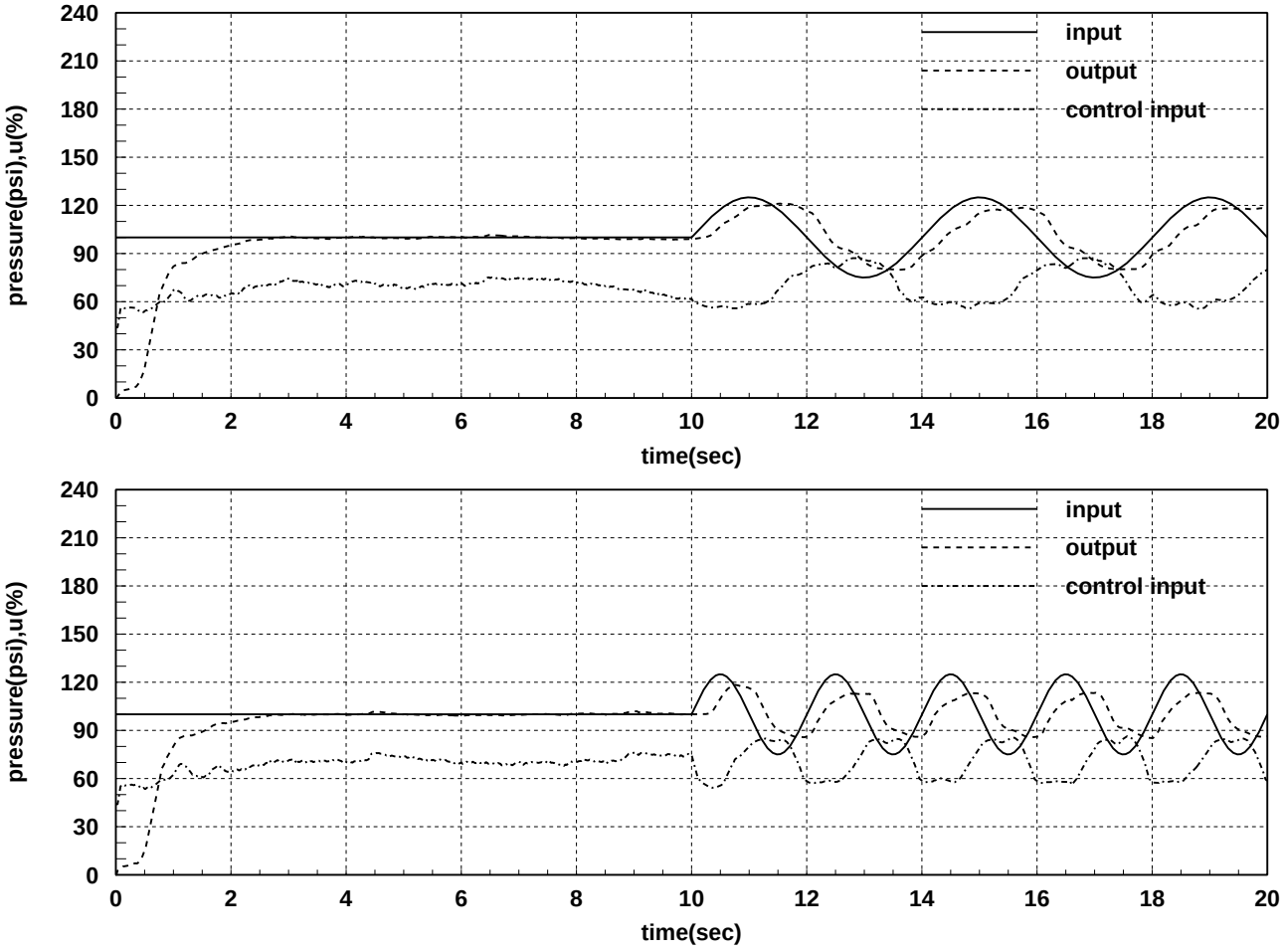

Figure 20: Closed loop system response for sinusoidal input of 0.25 Hz. (top) and 0.5 Hz. (bottom). The desired pressure is step input of 100 psi from 0 to 10 sec, from 10 sec to 20 sec a sinusoidal input with amplitude of 25 psi is superimposed on the step input. It should be noted that system bandwidth is around 0.5 Hz.

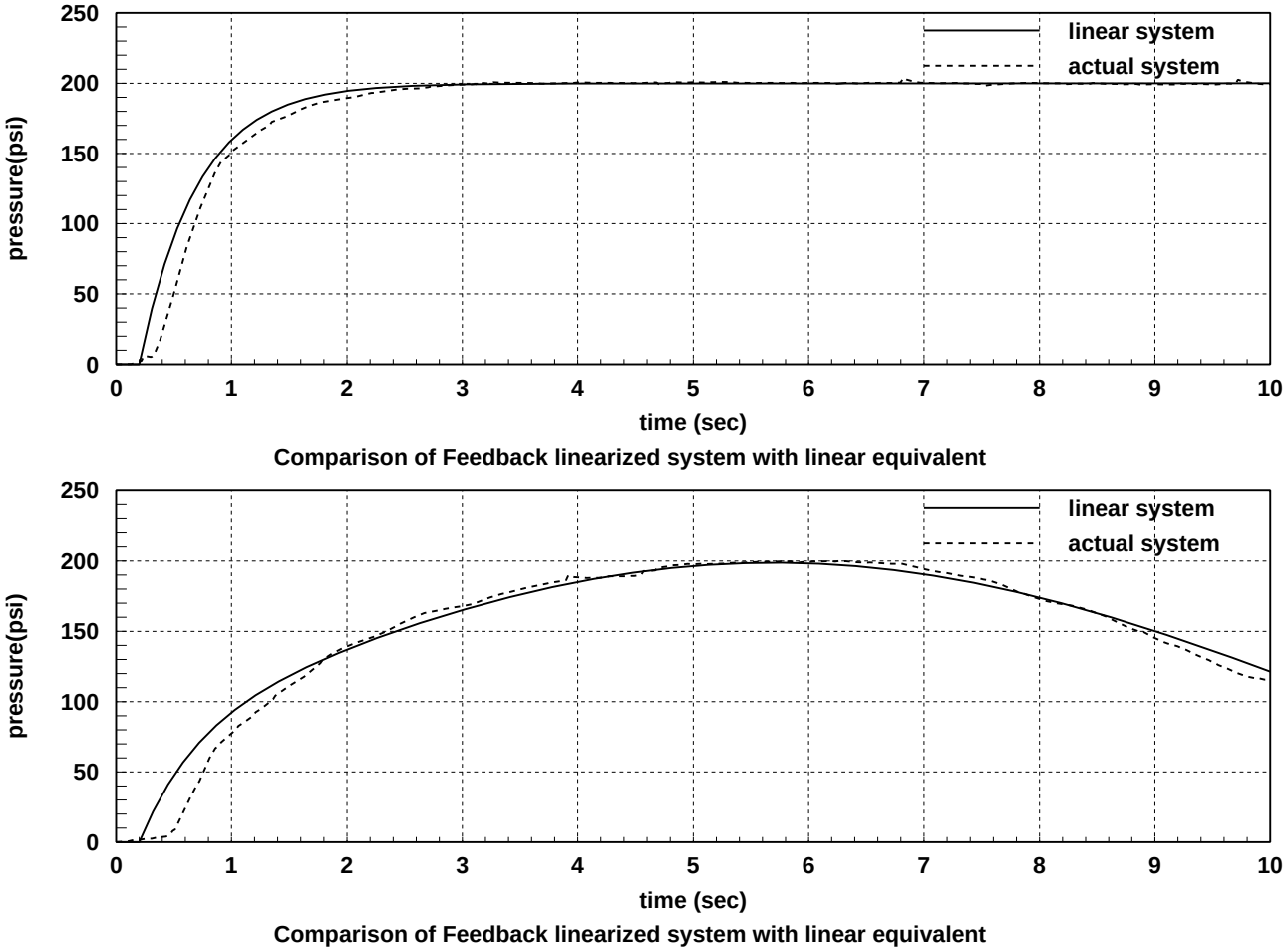

Figure 21: Comparison of the feedback linearized system response with the equivalent linear system response for two different inputs.